Broadband Photonic Integrated Transceiver Circuit for High-Range Resolution Frequency-Modulated Continuous-Wave Radar

Nabanita Sengupta, Marcel Grzeslo, Shuya Iwamatsu, Jonas Tebart, and Andreas Stöhr

Abstract – High-range resolution radar is essential for a variety of applications, including 3D imaging, target detection, spectroscopic material identification, and defense. In this article, to our knowledge, we report the first experimental validation of an instantaneous high-range resolution frequency-modulated continuous-wave (FMCW) terahertz radar that is based upon a photonic integrated circuit (PIC). The terahertz transceiver PIC consists of a unitraveling carrier photodiode terahertz transmitter monolithically integrated with a Fermi-level managed barrier diode (FMBD) terahertz receiver. In a proof-of-concept experiment, the FMCW terahertz radar PIC demonstrates being capable of detecting objects up to distances of 62.5 cm. For an FMCW bandwidth of 10 GHz, the measured range resolution is 14.5 mm. This is achieved by interconnecting the terahertz radar PIC to a conventional WR-3.4 horn antenna by using a ground-signal-ground probe. Finally, a fan-shaped bow-tie antenna is shown that allows increasing the FMCW bandwidth covering from 200 GHz to 600 GHz, resulting in a theoretical resolution below 1 mm.

1. Introduction

High-resolution target detection and imaging techniques using millimeter and terahertz waves are of significant importance in civil and security applications such as nondestructive testing, remote sensing, and object tracking [1, 2]. Terahertz frequency-modulated continuous-wave (FMCW) radar is an enabling technology for achieving high-resolution ranging due to the wide operational bandwidth available at terahertz frequencies.

Previously, it was shown that electronic and photonic terahertz FMCW radars offer high-range resolution at the millimeter level and even submillimeter level [1–9]. State-of-the-art electronic FMCW radar transceivers on the basis of 65 nm CMOS technology were reported to operate at 220 GHz to 320 GHz in [3], at 460 GHz to 520 GHz in [4], and at 450 GHz to 490 GHz in [5] using 90 nm SiGe BiCMOS technology. Although the FMCW bandwidth for electronic radars is typically limited at around 100 GHz [3, 6], photonic FMCW radars achieved much higher FMCW bandwidths of up to 4 THz [7–9]. In general, the higher FMCW bandwidth of photonic radars is associated with the beneficial use of frequency-downconverted wavelength-tunable lasers rather than frequency-upconverted electronically tunable oscillators. Although photonic terahertz radars can offer a much wider FMCW bandwidth and, thus, a higher range resolution to make them attractive for various system applications, a monolithically integrated photonic integrated circuit (PIC) for photonic terahertz radars has not been demonstrated, to our knowledge.

In this work, we present an InP-based monolithically integrated PIC for a terahertz FMCW radar front end. The fabricated PIC allows for ultrabroadband signal generation and detection with an operational bandwidth of several hundred gigahertz. The fabricated PIC consists of a 1.55 μm unitraveling carrier (UTC) photodiode (PD) for signal generation and a monolithically integrated Fermi-level managed barrier diode (FMBD) for downconverting the received radar signal to IF. In a proof-of-concept experiment, the developed terahertz radar PIC was connected to a WR-3.4 horn antenna by using a wafer probe. For an FMCW bandwidth of 10 GHz, the achieved range resolution is 14.5 mm. We also report on a broadband fan-shaped bow-tie antenna that can offer an FMCW bandwidth up to 400 GHz and can be monolithically integrated with the fabricated PIC.

2. Theory

In the FMCW radar, the frequency of the transmitted signal is swept over time. As the signal takes a certain time to travel to and from the target, the received signal is at a different frequency than what the transmitter is scattering at the time the reflected signal arrives back at the radar. By mixing the frequency of the two signals, the difference easily can be measured.

Radar range is the distance within which a radar system can detect objects by transmitting and receiving electromagnetic waves. Along with wavelength λ, the range mainly depends on the parameters given such as the transmitted power P_t, received power P_r, gain G of the antenna, and radar cross section σ. As σ also

Manuscript received 15 December 2024. This research was founded by the Ministry of Economic Affairs, Industry, Climate Action and Energy of the State of North Rhine-Westphalia within the project "5G.smart.Logport.Duisburg" (2108gif047a), the German Federal Ministry of Education and Research within "6GEM" (16KISK039), Open6GHub (16KISK017) and "6G ADLANTIK" (16KISK146), the German Research Foundation within "MARIE" (287022738–CRC/TRR 196, projects C06 and C07) and by the European Union Marie Skłodowska-Curie project "TERAOPTICS" (956857).

Nabanita Sengupta, Marcel Grzeslo, Shuya Iwamatsu, Jonas Tebart, and Andreas Stöhr are with the Department of Optoelectronics, University Duisburg–Essen, Lotharstraße 55, 47057 Duisburg, Germany; e-mail: nabanita.sengupta@uni-due.de, marcel.grzeslo@uni-due.de, shuya.iwamatsu@uni-due.de, jonas.tebart@uni-due.de, andreas.stoehr@uni-due.de.

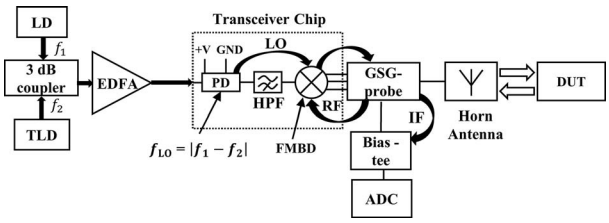

Figure 1. Schematic of terahertz FMCW radar setup (LD: laser diode; TLD: tunable laser diode; EDFA: erbium-doped fiber amplifier; and DUT: device under test).

depends on wavelength [10], it varies over a wide frequency range. The radar range equation calculates the maximum range of the radar, shown by

$$R_{\max} = \sqrt[4]{\frac{P_t \quad G^2\lambda^2 \quad \sigma}{P_r \quad (4\pi^3)}} \tag{1}$$

In addition, the ability to differentiate between two objects at different distances, also known as *range resolution*, is a crucial property of a radar system. The smallest measurable distance is determined by the bandwidth available within the system. Range resolution is given by

$$\text{Res} = \frac{c}{2 \ B} \tag{2}$$

where c is velocity of light at free space and B is the bandwidth of the system [11, 12]. As radar recognizes objects by the difference in distance, objects that are located at the same bearing as to the radar are reliably kept apart by the radar via distance detection. The distance estimation is based on IF and can be calculated as the following:

$$d = \frac{c \cdot f_{IF}}{2\left(\frac{df}{dt}\right)} \tag{3}$$

where $\frac{df}{dt}$ is the frequency shift per unit of time corresponding to the sweeping rate of the tunable source.

3. Conceptual System Design

The proposed system makes use of the InP-based terahertz PIC, where monolithically integrated UTC-PDs [13, 14] for generating power to transmit and

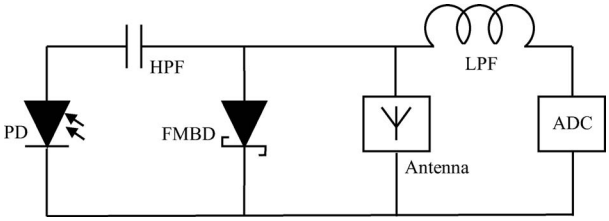

Figure 2. Simplified electrical equivalent circuit of the fabricated terahertz radar PIC.

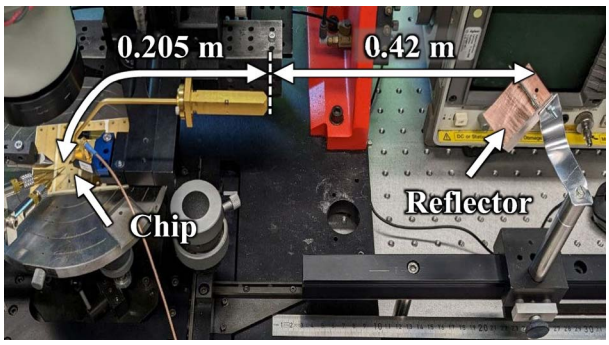

Figure 3. The terahertz FMCW radar measurement setup showing the probed mixer chip on the left and the sending and receiving signals from the target on the right.

FMBDs for mixing the received power from antenna are implemented together with a high-pass filter (HPF) for dc isolation [15]. For generating the ultrabroadband FMCW terahertz signal, an optical heterodyning system is exploited. The laser signal is compared with another reference laser that would have a fixed offset in frequency and phase. As most of the available systems have high losses at such high frequencies and low power range, stable heterodyne output is critical for obtaining stable output from this system. The output is then amplified and passed to the UTC-PD with optical fiber. The UTC-PD acts both as a local oscillator (LO) for the FMBD and transmitter sending the signal through an antenna toward the device under test. While receiving, the signal travels in the opposite direction, and the FMBD acts as receiver, as well as mixer. The IF output of the FMBD is then filtered through a low-pass filter and can be measured with an analog-to-digital converter (ADC).

4. FMCW Setup and Results

The transceiver chip was placed in a setup similar to Figure 1, and its performance was measured. One optical signal was generated at fixed wavelength by a highly stable laser (NKT Koheras BASIK X15), and the other was generated by a wavelength-tunable laser (Santec TSL-570). For the FMCW, a sawtooth modulation of the tunable laser with slope 1.24 THz/s was

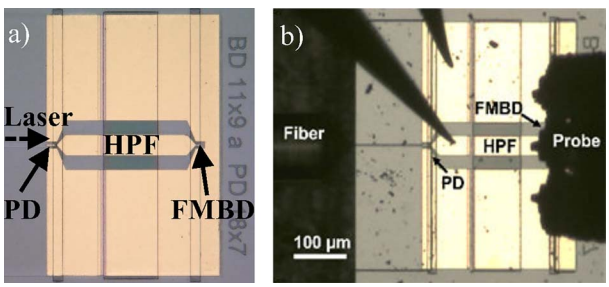

Figure 4. Close-up of the terahertz transceiver chip with (a) and without (b) probes and coupled lensed fiber.

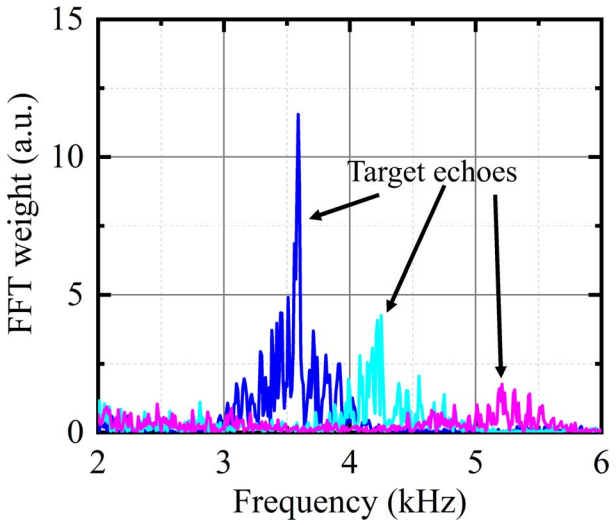

Figure 5. Measured signals mixed down by the FMBD receiver at the IF of ∼3.5 kHz (blue), ∼4.3 kHz (turquoise), and ∼5.3 kHz (pink) after object detection with the radar.

used, generating beat frequencies between 220 GHz and 330 GHz. The lights from the lasers were coupled to a 3 dB coupler to create an optical beat and amplified by an erbium-doped fiber amplifier. Afterward, the light was coupled to the UTC-PD on the InP substrate to generate a terahertz signal at the beat frequency. The output of the on-chip UTC-PD was extracted by ground-signal-ground (GSG) probe (Infinity probe, I325-T-GSG-100-BT, insertion loss ∼6 dB [14]) and transmitted to a target through a horn antenna (gain: 25 dBi). After the signal was reflected from the target, the signal was received by the same antenna and mixed in the on-chip FMBD with transmit signal acting as a LO, which was

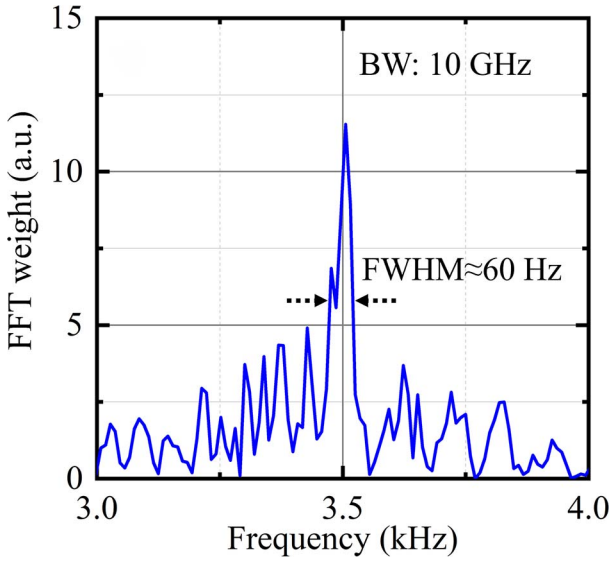

Figure 6. Target detection with sweeping bandwidth of 10 GHz (270 GHz to 280 GHz).

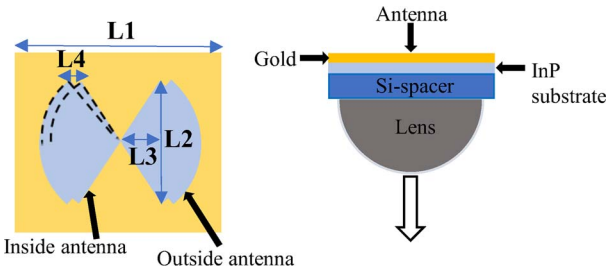

Figure 7. Fan-shaped bow-tie antenna and its placement.

directly fed by the on-chip UTC-PD, generating an IF output. The IF signal was extracted with the help of the integrated bias tee of the GSG probe. The distance of the target is calculated with the help of (3). Figure 2 represents the electrical equivalent of the circuit.

Figure 3 presents the measurement setup. For detecting the object, one corner reflector was placed at ∼0.21 m distance from the antenna head leading to a signal path of 0.42 m. Considering the guided propagation between the horn antenna and the on-chip mixer, the propagation path was around 0.2 m. This distance could be changed by moving the object on a rail. The close-up picture in Figure 4 depicts that UTC-PD was dc biased at −1 V by using dc needles, and the optical signal was transmitted via optical fiber coupling to the chip. The HPF prevented undesired biasing and irreversible damage in the FMBD from the generated photocurrent in the UTC-PD. The GSG probe on the right side contacted the coplanar waveguide pad for transmitting and receiving.

The wide bandwidth characteristics of FMBD were already explained in [16]. With a total distance of 62.5 cm, the IF was calculated to be ∼4.3 kHz. As shown in Figure 5, the object was detected at several distances of 42.5 cm, 52.5 cm, and 62.5 cm.

Figure 6 conveys the effect of bandwidth to precisely detect the target that is also associated with range resolution. The target placed at 0.425 m was measured with frequency ranging from 270 GHz to 280 GHz. The signal for 10 GHz B indicates a full width at half maximum (FWHM) of ∼60 Hz corresponding to a calculated resolution of 14.5 mm, which is in good agreement with the theoretical value of 15 mm, according to (2). To show an improved resolution for higher BWs, it is necessary to reduce the influence of the laser's sweeping nonlinearity. Also, it should be confirmed that the resolution is not limited due to the frequency noise of the laser.

Table 1. Fan-shaped bow-tie antenna dimensions

Dimension	Unit (μm)
L1	650
L2	125
L3	200
L4	75

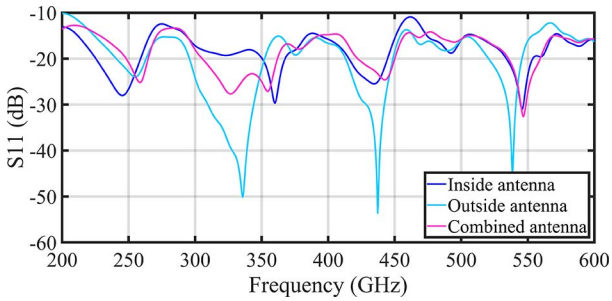

Figure 8. The simulated S_{11} of the presented fan-shaped slot bow-tie antenna for the different number of arcs overlapped.

5. Next Step of Integration: Antenna

For implementing an integrated on-chip radar system, a wideband antenna needs to be combined with the transceiver. A slot bow-tie antenna known for its wideband response is a promising candidate. Due to its planar structure, monolithic integration with the transceiver is possible. A fan-shaped slot bow-tie antenna [17] is designed on the InP substrate, and its characteristics are investigated by 3D electromagnetic wave simulation (CST Microwave Studio, version CST Studio Suite 2023). The schematic of the designed antenna is presented in Figure 7. The antenna dimensions, which are optimized to obtain an operational bandwidth covering from 200 GHz to 600 GHz, are shown in Table 1.

A discrete excitation port is placed at the center of the antenna for simulating the S parameter (S_{11}) and the radiation properties. The antenna is placed on an Si hemispherical lens with a radius of 2 mm to collimate the beam. The lens allows extracting terahertz output power from the backside of the high-permittivity InP substrate, resulting in an increase of antenna gain. By inserting an Si spacer with 500 μm thickness between the antenna chip and the lens, the gain is further enhanced [17].

The antenna is made by overlapping two bow-tie antennas together. First, a fan-shaped antenna having only a single arc is designed. The simulated S parameters (S_{11}) with values below -10 dB are shown in Figure 8. For improving the performance at all frequencies, an additional antenna with increased radius is overlapped.

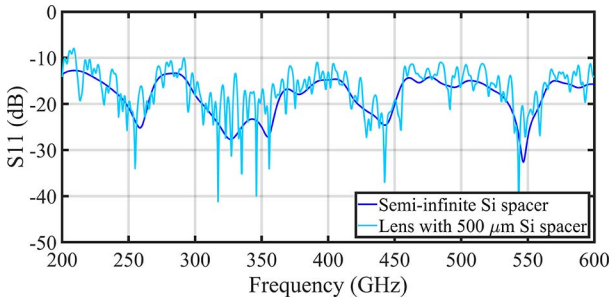

Figure 9. Comparison of simulated S_{11} of the presented fan-shaped slot bow-tie antenna in the presence of the semi-infinite Si spacer and lens with the 500 μm spacer.

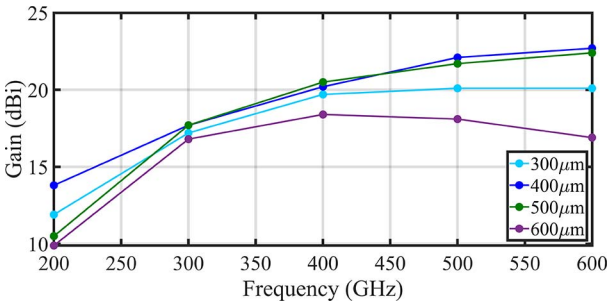

Figure 10. Gain over frequency range for different spacer thicknesses of the presented bow-tie antenna.

As a result, the S_{11} over the whole frequency range is decreased to around -15 dB. With an increased number of antennas, reflection loss throughout the frequency range is achieved. During simulation, the antenna is placed on a semi-infinite Si spacer. The simulated result of S_{11} this way is equivalent to placing the antenna on a lens together with Si spacer of 500 μm [19]. Figure 9 supports the result of enabling a time-efficient antenna design.

To increase the gain, the antenna is placed on a lens of 2 mm radius with different spacer thicknesses in between. The Si thicknesses considered for simulations are 300 μm, 400 μm, 500 μm, and 600 μm. Figure 10 plots the simulated antenna gains along the frequency range for different spacer thicknesses.

The antenna achieves the best performance for the 400 μm thick spacer, with a hemispherical Si lens of 2 mm radius. The simulated highest gain is 22.7 dBi at 600 GHz for the 400 μm thick spacer.

Figure 11 shows the simulated radiation pattern of the antenna at the center frequency of 400 GHz for the 400 μm spacer. The projected beam is focused at 180°. In other words, most of the power is focused downward. As a result, the range of radar could be further increased. It makes this antenna favorable for radar applications.

6. Conclusion and Outlook

The first terahertz FMCW radar front-end PIC featuring an ultrabroadband UTC-PD transmitter monolithically integrated with the FMBD acting as a terahertz mixer is reported. In a proof-of-concept experiment, a range resolution of 14.5 mm is achieved for the 10 GHz FMCW bandwidth. The current setup is limited with respect to the operational bandwidth

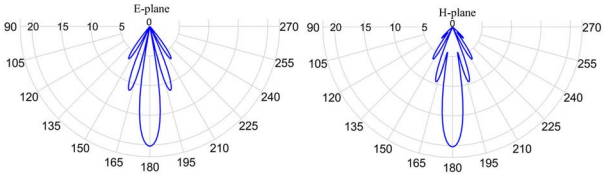

Figure 11. The E-plane (left) and H-plane (right) radiation pattern of the presented bow-tie antenna at 400 GHz for 400 μm spacer; gain (decibels isotropic) versus angle (degree).

that could be overcome by integrating the PIC with a planar bow-tie antenna that potentially leads to FMCW bandwidths of several hundred gigahertz.

7. References

1. L. Yi, Y. Li, and T. Nagatsuma, "Photonic Radar for 3D Imaging: From Millimeter to Terahertz Waves," *IEEE Journal of Selected Topics in Quantum Electronics*, **29**, 5, July 2023, pp. 1-14.
2. Y. Monnai, X. Lu, and K. Sengupta, "Terahertz Beam Steering: From Fundamentals to Applications," *Journal of Infrared, Millimeter, and Terahertz Waves*, **44**, February 2023, pp. 169-211.
3. X. Yi, C. Wang, X. Chen, J. Wang, J. Grajal, et al., "A 220-to-320-GHz FMCW Radar in 65-nm CMOS Using a Frequency-Comb Architecture," *IEEE Journal of Solid-State Circuits*, **56**, 2, February 2021, pp. 327-339.
4. C. Mangiavillano, A. Kaineder, and A. Stelzer, "A 0.46–0.52-THz Fully-Differential Quasi-Monostatic FMCW Radar Transceiver in 90-nm SiGe BiCMOS," *e+i Elektrotechnik und Informationstechnik*, **141**, 1, December 2023, pp. 3-10.
5. C. Mangiavillano, A. Kaineder, K. Aufinger, and A. Stelzer, "A 1.42-mm^2 0.45–0.49 THz Monostatic FMCW Radar Transceiver in 90-nm SiGe BiCMOS," *IEEE Transactions on Terahertz Science and Technology*, **12**, 6, November 2022, pp. 592-602.
6. X. Yi, C. Wang, M. Lu, J. Wang, J. Grajal, et al., "A Terahertz FMCW Comb Radar in 65nm CMOS with 100GHz Bandwidth," 2020 IEEE International Solid-State Circuits Conference, San Francisco, CA, USA, February 16–20, 2020, pp. 90-92.
7. L. Liebermeister, S. Nellen, R. B. Kohlhaas, S. Lauck, M. Deumer, et al., "Optoelectronic Frequency-Modulated Continuous-Wave Terahertz Spectroscopy With 4 THz Bandwidth," *Nature Communications*, **12**, February 2021, p. 1071.
8. L. Yi, R. Kaname, R. Mizuno, Y. Li, M. Fujita, et al., "Ultra-Wideband Frequency Modulated Continuous Wave Photonic Radar System for Three-Dimensional Terahertz Synthetic Aperture Radar Imaging," *Journal of Lightwave Technology*, **40**, 20, October 2022, pp. 6719-6728.
9. F. Zhang, Q. Guo, and S. Pan, "Photonics-Based Real-Time Ultra-High-Range-Resolution Radar With Broadband Signal Generation and Processing," *Scientific Report*, **7**, 13848, October 2017, p. 13848.
10. C. Buchberger, F. Pfeiffer, and E. Biebl, "Dielectric Corner Reflectors for mmWave Applications," *Advances in Radio Science*, **17**, September 2019, pp. 197-203.
11. M. N. Cohen, "An Overview of High Range Resolution Radar Techniques," National Telesystems Conference Proceedings, Atlanta, GA, USA, March 26–27, 1991, pp. 107-115.
12. H. Weidong, Z. Xu, Z. Han, H. Jiang, Y. Liu, et al., "Ultra-Wideband Signal Generation and Fusion Algorithm for High-Resolution Terahertz FMCW Radar Imaging," *Optics Express*, **30**, 6, March 2022, pp. 9814-9822.
13. M. Grzeslo, S. Dülme, S. Clochiatti, T. Neerfeld, T. Haddad, et al., "High Saturation Photocurrent THz Waveguide-Type MUTC-Photodiodes Reaching mW Output Power Within the WR3.4 Band," *Optics Express*, **31**, 4, February 2023, pp. 6484-6498.
14. S. Iwamatsu, M. Ali, J. L. F. Estévez, M. Grzeslo, S. Makhlouf, et al., "Terahertz Photodiode Integration With Multi-Octave-Bandwidth Dielectric Rod Waveguide Probe," *Optics Letters*, **48**, 23, December 2023, pp. 6275-6278.
15. M. Grzeslo, A. Lavrič, T. Brüning, J. Tebart, S. Iwamatsu, et al., "Monolithically Integrated Optically Pumped InP-Based THz Mixer," 48th International Conference on Infrared, Millimeter, and Terahertz Waves, Montreal, QC, Canada, September 17–22, 2023, pp. 1-2.
16. N. Sengupta, M. Grzeslo, S. Iwamatsu, J. Tebart, T. Haddad, et al., "Ultra-Broadband Photonic THz Transceiver IC for High Range Resolution FMCW RADAR," 2024 4th URSI Atlantic Radio Science Meeting, Grand Canary Island, Spain, May 19–24, 2024, pp. 1-4.
17. R. G. L. de Mello, A. C. Lepage, and X. Begaud, "The Bow-Tie Antenna: Performance Limitations and Improvements," *IET Microwaves, Antennas and Propagation*, **16**, 5, March 2022, pp. 283-294.
18. D. F. Filipovic, S. S. Gearhart, G. M. Rebeiz, "Double-Slot Antennas on Extended Hemispherical and Elliptical Silicon Dielectric Lenses," *IEEE Transactions on Terahertz Science and Technology*, **41**, 10, October 1993, pp. 1738-1749.
19. K. Rasilainen, J. Chen, M. J. Nokandi, S. P. Singh, M. E. Leinonen, et al., "Over-the Air Characterization of a Steerable Sub-THz Si Lens and On-Chip Antenna System," *IEEE Transactions on Microwave Theory and Techniques*, **72**, 5, May 2024, pp. 2883-2898.